Electrostatic instability of micro-plates subjected to differential pressure
A semi-analytical approach

Sajadi, Banafsheh; Goosen, Hans; van Keulen, Fred

DOI
10.1016/j.ijmecsci.2018.02.007

Publication date
2018

Document Version
Final published version

Published in
International Journal of Mechanical Sciences

International Journal of Mechanical Sciences 138–139 (2018) 210–218

Contents lists available at ScienceDirect

International Journal of Mechanical Sciences

journal homepage: www.elsevier.com/locate/ijmecsci

Electrostatic instability of micro-plates subjected to differential pressure: A semi-analytical approach

Banafsheh Sajadi*, Hans Goosen, Fred van Keulen

Department of Precision and Microsystem Engineering, Delft University of Technology, Delft, 2628 CD, The Netherlands

ARTICLE INFO

Keywords:
Pull-in
Electrostatic instability
Bi-stability
Micro-plate
Snap-through
Nonlocal elasticity

ABSTRACT

Electrostatic instability is one of the main features of many electrostatic MEMS and NEMS devices. In this paper, we investigate how the electrostatic instability of a plate-like electrode can be affected by a differential pressure. The results of this study indicate that the presence of differential pressure can have a significant influence on the equilibrium path, the number and location of unstable points, and the post-instability behavior. As a result, while the system is loaded and unloaded electrically, the electrostatic instability might lead to a snapping behavior. The noticed snapping behavior of a flat plate makes it very appealing for sensing and actuating applications. This study is based on both a semi-analytical framework and finite element simulations. The proposed analytical solution is shown to be accurate enough to be used as an effective tool for design.

1. Introduction

Electrostatic instability (and bi-stability) is an important feature of many electrostatic MEMS devices, sensors and actuators [1–3]. A solid understanding of the electrostatic instability is essential to improve the performance such MEMS/NEMS devices and to obtain new designs for new applications.

Electrostatic MEMS devices essentially consist of a simple parallel plate capacitor with at least one flexible electrode. When an electric potential is applied to the capacitor, an attractive electrostatic load is induced between its electrodes. This load depends on the applied electric potential, the local distance between the electrodes, and the dielectric constant of the medium separating them [4]. The electrostatic load leads to deformation of the flexible electrode(s) to maintain the balance between electrostatic and elastic potentials. Thus, any small change in the electric potential can generate mechanical movement of the flexible plate, which can be used for actuation [5].

Instability of an electrostatic MEMS device occurs mainly due to the nonlinearity in the electrostatic potential [6]. When the system becomes unstable, any perturbation could lead to failure or pull-in of the flexible electrode. This stability phenomenon appears as a fold or a limit point in the equilibrium curve of the system [7,8].

In certain electrostatic MEMS devices, e.g. microphones and pressure sensors or actuators, it is essential to avoid pull-in effects, since the contact between the two electrodes induces failures, including short circuit, stick, wear, dielectric changing, and breakdown [6,9]. On the other hand, pull-in is a feature of MEMS/NEMS devices [2] which can also provide information on the mechanical and physical characteristics of the system. Therefore, it has been introduced as a robust mechanism for measuring the mechanical properties of nano-structures [10], or sensing the adsorbate stiffness in nano-mechanical resonators [11].

In order to avoid or employ the pull-in effect, an in-depth knowledge of the stability behavior and an accurate determination of the pull-in voltage of the structure is critically required. In engineering applications, to approximate the critical deformation of the electrode and to predict the pull-in voltage, a simple 1-D spring-mass model is commonly used (see Fig. 1). In such a model, the instability occurs when due to the deformation of the flexible electrode, the gap between the two electrodes becomes two thirds of the initial gap [7,12,13]. This simplified model is commonly referred to as the '1/3 air gap rule'. In practice, however, a membrane/plate structure is different from a simple spring mass model. It is a 2D structure which incorporates Poisson ratio effects, and membrane stiffening effects. In addition, if the plate-like electrode deforms, the electrostatic load is no longer uniform. The 1/3 air gap model inherently does not account for any of these effects. However, the critical gap being equal to two-thirds of the initial gap size, is shown to be the most conservative critical gap in MEMS capacitors [12].

The pull-in of circular clamped plate-like electrodes has been investigated and formulated in many studies [9,12,14]. These studies are based on simplifying assumptions, such as small and one-dimensional defor-

* Corresponding author.
E-mail address: b.sajadi@tudelft.nl (B. Sajadi).

https://doi.org/10.1016/j.ijmecsci.2018.02.007
Received 12 June 2017; Received in revised form 3 January 2018; Accepted 3 February 2018
Available online 6 February 2018

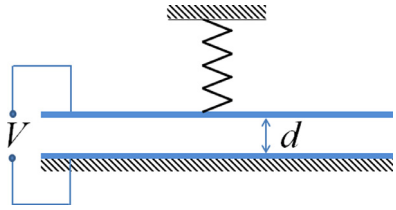

Fig. 1. Simple 1-D model typically used to approximate the critical deformation of the electrode in order to predict the pull-in voltage.

mation of the plate, or uniformity of the electrostatic load. Ultimately, finite-difference and finite-element methods have been applied to solve the resulted equations [9,15,16]. Different values for critical deformation were proposed for circular clamped electrodes, from 41.5% [9] or 41.6–45.6% [15] to 72–75% [16] depending on the thickness of the plate and simplifying assumptions. However, a comprehensive *analytical* solution for pull-in voltage of a circular clamped plate, while considering the nonlinear membrane effects and non-uniformity of electrostatic load, is missing in the literature.

The pull-in voltage and critical deflection of cantilever-, beam- or plate-like electrodes depend on the stiffness of the flexible component, as well as the initial distance between the electrodes. A mechanical load applied to the component can directly affect both parameters, and consequently, influences the electrostatic instability of the system. The sensitivity of electrostatic instability to a mechanical load is the concept behind using pull-in instability as a mechanism for sensing, for example, temperature [17], surface-stress [4], or residual stresses in clamped structures [7]. Furthermore, MEMS sensors and actuators are frequently designed to operate under a mechanical load, such as in capacitive pressure sensors. Sometimes, the additional mechanical load in these devices is undesired, but also inevitable, such as thermal loads or residual stresses in clamped structures. Therefore, an in-depth knowledge about the effect of these mechanical loads on the stability of the micro mechanical component is paramount.

The dependency of the pull-in voltage of MEMS devices to external mechanical loads, such as a uniform transverse, or, in-plane load, has been investigated in the literature [7,13,18–22]. Particularly, the effect of a uniform differential pressure on the electrostatic instability of a circular micro plate has been studied as well [23]. The later, using a numerical continuation scheme, calculated the combination of pressure and voltage which can lead to the instability of the system. This study considers the differential and the electrostatic pressure to be in the same direction and it shows that the differential pressure always causes the system to be more prone to instability. It should be noticed that the proposed numerical method, even if highly accurate, is an expensive tools, and, for each new set of design parameters (radius or thickness) the simulation has to be repeated. An accurate analytical model –if available– could provide a closed form solution for approximating the pull-in voltage and the critical deformation almost without any time cost. In addition, it provides more insight to the problem which is favored for design purposes.

In this paper, we propose an analytical approximate methodology to study the stability and pull-in behavior of a circular flexible electrode, while, loaded with electrostatic and differential pressure. In this analysis, the direction of the pressure is not predefined. Instead, it is considered to be a differential pressure positive when opposing the electrostatic load, and negative otherwise. The non-linear stretching of the thin plate and the non-uniformity of electrostatic load due to deflection of the flexible plate, are incorporated in this solution. The accuracy of the proposed analytical approximation is evaluated with a comparison to the finite element simulations [24].

Using the proposed solutions, first, the instability and pull-in behavior of the electrode and its dependency on the electrode's thickness and radius are discussed. Next, we explore how a differential pressure and its direction would affect equilibrium, stability, and the critical voltages and deflections. In addition, the post-instability behavior of the system

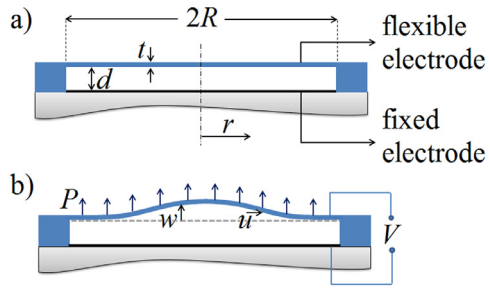

Fig. 2. Schematic of the cross section of the capacitor with one flexible electrode in a) undeformed configuration, and, b) deformed under combined electrostatic and differential pressure.

and possible snapping behavior will be addressed. We will show that the presence of a differential pressure can trigger bi-stability in the system. The required criteria to attain the additional stable solution and the snapping behavior, which can be of great interest for sensing and actuation purposes, will be thoroughly discussed.

Finally, we shall remind that the effective elastic properties of structures at nano and sometimes even at micro scales are known to be strongly size-dependent [25–29]. The classical continuum theory is inherently size in-dependent and hence, it cannot provide a good prediction when the thickness of the plate is very small. For small length scales, size-dependent continuum theories that account for these scale effects should be utilized [30–36]. These theories, embed a material length scale ($e_0 a$) which makes it possible to qualify the size of a structure as large" or small" relative to its material length scale. If the size of the structure is relatively large, then the nonlocal or higher-order gradient theories converge to classical elasticity theory and therefore, employing the classical theory will lead to similar results. Once plasticity plays a role, another length scale should be considered [37]. In this paper, using a strong nonlocal elasticity theory [35,38], the possibility of capturing the scaling effects in the proposed formulation is briefly investigated, and the size-dependence of stability of a micro-plate while subjected to electrostatic and differential pressure is addressed.

2. Analytical formulation

The analytical model proposed here is based on a parallel plate capacitor with a thin, circular, fully clamped plate as one electrode, while the other is fixed and rigid. The shape of the capacitor is chosen to be circular, since the MEMS devices with a circular plate generally yield better structural flexibility as compared to rectangular plates. In addition, they have no corners or sharp edges which may induce high residual stresses during fabrication process [15]. The schematic of the assumed model is shown in Fig. 2.

The radius of the flexible electrode is R and its thickness is h. It is modeled with a linear elastic, homogeneous and isotropic material model. The Youngs modulus and Poisson ratio of the plate are denoted E and ν, respectively. The plate is suspended over the grounded electrode with similar radius and the initial gap between the electrodes is d. The plate is loaded with a differential pressure P, and an electric potential V is applied to the electrodes.

The plate is modeled with von Kármans plate theory, which accounts for finite deflection but moderate rotations and is adequate for thin plates [39]. The loads are conservative, which implies that first, to estimate the deflection in the equilibrium state, approximations based on minimizing the total potential energy can be applied, and second, no dynamic consideration is required to assess stability of equilibriums. Minimizing the total potential energy is a variational problem and its solution can be estimated using Ritz's method. In this method a parametrized displacement field satisfying the clamping boundary condition is considered, whereas the unknown parameters are calculated by requiring the total potential energy to be stationary.

Due to the axisymmetric condition in the problem at hand, the only appearing displacement components are the radial (u) and transverse (w) components. Although, the nonlinearity might cause the symmetry to break up, we consider the symmetry to maintain during deformation. This assumption has been verified using a finite element model which will be described in the next section. The clamping boundary condition forces the displacement components and also the first derivative of the transverse displacement with respect to the radial coordinate to be equal to zero at the boundaries. We adopt Timoshenko's simple approximate displacement field for uniformly loaded circular plates [40], to approximate the radial (u) and transverse (w) displacements:

$$w = C_1 d(1-\rho^2)^2,$$
$$u = R\rho(1-\rho)(C_2 + C_3\rho), \tag{1}$$

where $\rho = \frac{r}{R}$ is the non-dimensional radial coordinate and, C_i, (i= 1–3,) are the parameters to be calculated. Next, the associated total potential energy is evaluated. The total potential energy consists of four terms namely, the electrostatic potential (U_e), the potentials associated with elastic deformation due to the bending (U_b) and the stretching (U_s) of the plate, and the potential associated with the mechanical pressure (W):

$$U = U_e + U_b + U_s - W. \tag{2}$$

Assuming the parallel-plate capacitor theory, the electrostatic potential follows as [2,41]:

$$U_e = -\pi\epsilon V^2 R^2 \int_0^1 \frac{\rho d\rho}{d+w}, \tag{3}$$

where ϵ is the electric permittivity of the dielectric between the electrodes. Notice that the local distance between the electrodes $(d + w)$ is employed to calculate the electrostatic potential. Thus, the non-uniformity of the electrostatic load due to the deflection of the flexible electrode is incorporated.

Provided that the micro-plate is isotropic and homogeneous, the bending-extension coupling stiffness equals to zero. Therefore, the potentials associated with elastic deformation can be decoupled to the bending energy (U_b) and the stretching energy (U_s) [39]:

$$U_b = \frac{\pi D}{R^2}\int_0^1 \left(\left(\frac{\partial^2 w}{\partial\rho^2}\right)^2 + \left(\frac{1}{\rho}\frac{\partial w}{\partial\rho}\right)^2 + \left(\frac{2\nu}{\rho}\frac{\partial w}{\partial\rho}\frac{\partial^2 w}{\partial\rho^2}\right)\right)\rho d\rho, \tag{4a}$$

$$U_s = \frac{\pi Eh}{(1-\nu^2)}\int_0^1 \left(\left(\frac{u}{\rho}\right)^2 + \left(\frac{\partial u}{\partial\rho} + \frac{1}{2R}\left(\frac{\partial w}{\partial\rho}\right)^2\right)^2 + \frac{2\nu u}{\rho}\left(\frac{\partial u}{\partial\rho} + \frac{1}{2R}\left(\frac{\partial w}{\partial\rho}\right)^2\right)\right)\rho d\rho, \tag{4b}$$

where $D = \frac{Eh^3}{12(1-\nu^2)}$ is the bending stiffness of the flexible plate. Notice that nonlinear membrane effects have been incorporated in the elastic potential.

As the rotations in the plate due to mechanical and electrostatic loads are small, the pressure is assumed to be always perpendicular to the undeformed surface. Therefore, the potential associated with the pressure can be calculated as:

$$W = 2\pi P R^2 \int_0^1 w\rho d\rho. \tag{5}$$

By substituting Eq. (1) into Eqs. (3)–(5), an approximation for the total potential energy can be derived analytically. Since the analytical expression of the integral in Eq. (3), depends on the sign of the parameter C_1, we shall calculate the total potential energy and solve the problem for $C_1 < 0$ and $C_1 > 0$, separately:

$$U = -\epsilon V^2 \frac{\pi R^2}{2d}\left(F(C_1)\right) - P\frac{\pi R^2 d}{3}C_1 + \frac{32\pi d^2}{3R^2}DC_1^2 + \frac{EhR^2\pi}{(1-\nu^2)}\left(\alpha_1 C_2^2 + \alpha_2 C_3^2 + \alpha_3 C_2 C_3 - \alpha_4 C_1^2 C_2\frac{d^2}{R^2} + \alpha_5 C_3 C_1^2\frac{d^2}{R^2} + \alpha_6 C_1^4\frac{d^4}{R^4}\right), \tag{6}$$

where, α_i is introduced for compactness, with $\alpha_1 = 0.250$, $\alpha_2 = 0.117$ $\alpha_3 = 0.300$, $\alpha_4 = 0.068$, $\alpha_5 = 0.055$, $\alpha_6 = 0.305$. These parameters are determined by the selected basis-functions, and represent the linear and nonlinear stretching stiffness components in the strain energy. Moreover,

$$F(C_1) = \frac{\operatorname{atanh}\sqrt{-C_1}}{\sqrt{-C_1}} \qquad \text{if } C_1 < 0, \tag{7a}$$

$$F(C_1) = 1 \qquad \text{if } C_1 = 0, \tag{7b}$$

$$F(C_1) = \frac{\operatorname{atan}\sqrt{C_1}}{\sqrt{C_1}} \qquad \text{if } C_1 > 0. \tag{7c}$$

Notice that $F(x)$ is a continuous and smooth function around zero. Next, the stationary points of total potential energy (U) can be found by equating its derivative to the unknown parameters (C_i) to zero,

$$\frac{\partial U}{\partial C_1} = \frac{\partial U}{\partial C_2} = \frac{\partial U}{\partial C_3} = 0. \tag{8}$$

Solving Eq. (8) for parameters C_2 and C_3, leads to a relation between the stretching of the electrode and its transverse deflection, independent of the applied loads, V and P. As a matter of fact, C_2 and C_3 can be calculated as a function of C_1 and substituted into Eq. (6). Hence, the degrees of freedom can be reduced to C_1 only, while incorporating the in-plane deformation, as well. Then, equilibrium requires:

$$\frac{\partial U}{\partial C_1} = 0, \tag{9}$$

which leads to:

$$-\epsilon V^2\frac{\pi R^2}{2d}\left(\frac{1}{2C_1(1+C_1)} - \frac{F(C_1)}{2C_1}\right) + \frac{64\pi}{3}\left(\frac{d}{R}\right)^2 D\left(C_1 + 0.488\left(\frac{d}{h}\right)^2 C_1^3\right) - P\frac{\pi R^3}{3}\frac{d}{R} = 0. \tag{10}$$

It is worth to note that in Eq. (10), two sources of nonlinearity are incorporated: (1) the cubic term due to the geometrical nonlinearity and, (2) the nonlinearity of electrostatic load. Due to the presence of nonlinearity, multiple equilibrium states might be found for one load case (P and V). Therefore, the equilibrium path might exhibit one or even more bifurcations, at which solution branches meet. The stability of the solution can be defined by the sign of the second derivative of the total potential energy with respect to the only degree of freedom left (C_1). In fact, the system is stable, when the second derivative is positive, and unstable, if it is negative.

The critical point(s) can be calculated by equating the second derivative of the total potential energy with respect to the only degree of freedom to zero. This, from a physics point of view, means that the system would have no stiffness in the direction of the subjected degree of freedom. Therefore, the second derivative of the total potential energy at the critical points can be calculated as:

$$\frac{\partial^2 U}{\partial {C_1}^2} = -\epsilon V^2\frac{\pi R^2}{2d}\left(-\frac{5C_1+3}{4(C_1+1)^2 {C_1}^2} + \frac{3F(C_1)}{4{C_1}^2}\right) + \frac{64\pi d^2}{3R^2}D\left(1 + \alpha_7\left(\frac{d}{h}\right)^2 {C_1}^2\right) = 0. \tag{11}$$

where $\alpha_7 = 1.464$.

Recall that at the critical points, the system is still in equilibrium. Thus, Eqs. (10) and (11) should be solved simultaneously in order to calculate the critical deflection(s) and voltage(s). The critical value of voltage and deflection are denoted with superscribe *cr*. With such an analytical solution, one can accurately approximate the voltage level(s) at which instability occurs as a function of the material properties, the geometrical parameters, and the applied differential pressure. It is worth noting that since Eqs. (10) and (11) are both highly nonlinear in C_1, solving these equations numerically is relatively difficult. Therefore, as an alternative, one can simply solve these equations for P and V for a feasible range of critical C_1^{cr} (e.g. -0.99 to +1). This approach will result in obtaining C_1^{cr} as a numeric function of P and V.

3. Finite element analysis

To verify the results of the analytical estimation, a 3D circular electrode was modeled using finite elements (COMSOL Multiphysics [24]). In the model, the electrode is considered to be flexible, clamped on the edge and it was discretized with solid elements using free tetrahedral meshing. The material properties and specifications of the model, that are used for the test case for this solution, are: $E = 80$ GPa, $\nu = 0.2$, $\epsilon = 8.854 \times 10^{-12}$ $m^{-3}kg^{-1}s^4$ A^2 and $d = 2$ μm. To study the effect of the dimensions of the electrode, different combinations of thickness and radius have been studied.

The electrostatic and differential pressures have been applied as boundary loads to the plate, as P and $\epsilon \frac{-V^2}{2(d+w)^2}$, where w is the transverse displacement field of the micro-plate and V is a variable representing the voltage. In the solid mechanics module, a global equation is introduced to define the voltage (V) as a function of the average deflection of the plate. Hence, the required electric potential to maintain the equilibrium of the plate for a specified average deflection (w_0) can be calculated.

This calculation is repeated over a range of average deflections and as a result, the equilibrium path of the system is achieved. It should be noticed that in the finite element model, the symmetry of the displacement field is not imposed to the system. However, the displacement field appears to be axi-symmetric for both the resulting stable and unstable solution branches. The results from this model is compared with the proposed analytical solution in the "Results and discussion".

4. Scaling effects

In order to use the formulation proposed in Section 2 for design purposes, one should consider a thickness range at which the elastic coefficients for bulk materials can still be employed. Otherwise, a proper size dependent theory shall be employed to capture the scale effects in the formulation.

Here, we briefly discuss the scaling effects on the obtained formulation using a strong nonlocal plate formulation [38,42,43]. Assuming that the radius of the plate is much larger than its thickness, and the stress derivatives in radial direction are small, we can neglect the nonlocal effects in in-plane direction. Therefore, the scaling modification factor provided by Ref. [35] can be adopted for imposing the scaling effects on the bending and stretching rigidities of the plate as a function of its thickness:

$$\lambda = \frac{1}{\eta\sqrt{\pi}}\left(\exp(-\eta^2) - 1\right) + \operatorname{erf}(\eta), \tag{12}$$

and,

$$\beta = \operatorname{erf}(\eta) - \frac{1}{\sqrt{\pi}}\left(\frac{2}{\eta}\exp(-\eta^2) + (3\eta^{-1} - 2\eta^{-3})(1 - \exp(-\eta^2))\right). \tag{13}$$

where erf is the error function, $\eta = \frac{h}{e_0 a}$ as $e_0 a$ is the material length scale, and the obtained λ and β are the modification factors for stretching and bending rigidities, respectively. These factors are obtained by using a three dimensional strong nonlocal formulation and a Gaussian nonlocal kernel for a plate of which the radius is much larger than the thickness. More details of the derivation of these factors can be found in Ref. [35].

As a consequence of employing these factors, the stretching and bending energy terms in Eqs. (4b) and (4a) can be modified. Following the procedure as discussed in Section 2 results in equilibrium and instability conditions:

$$\begin{aligned}\frac{\partial U}{\partial C_1} &= -\epsilon V^2 \frac{\pi R^2}{2d}\left(\frac{1}{2C_1(1+C_1)} - \frac{f(C_1)}{2C_1}\right) \\ &+ \frac{64\pi}{3}\left(\frac{d}{R}\right)^2 D\left(\lambda C_1 + 0.488\beta\left(\frac{d}{h}\right)^2 C_1^3\right) \\ &- P\frac{\pi R^3}{3}\frac{d}{R} = 0.\end{aligned} \tag{14}$$

$$\begin{aligned}\frac{\partial^2 U}{\partial {C_1}^2} &= -\epsilon V^2 \frac{\pi R^2}{2d}\left(-\frac{5C_1+3}{4(C_1+1)^2 {C_1}^2} + \frac{3f(C_1)}{4{C_1}^2}\right) \\ &+ \frac{64\pi d^2}{3R^2} D\left(\lambda + \alpha_7\beta\left(\frac{d}{h}\right)^2 {C_1}^2\right) = 0.\end{aligned} \tag{15}$$

In order to obtain the size dependent critical deflection(s) and voltage(s), Eqs. (14) and (15) should be solved simultaneously. In the next section, we will briefly discuss the effects of using the proposed formulation, and capturing the scaling effects, on the stability assessment of a micro-plate while subjected to differential and electrostatic pressures.

5. Results and discussion

In this section, the influence of a uniform pressure on the critical deflection and voltage of a parallel plate capacitor with a circular flexible electrode, will be studied. The results of the proposed analytical approximation will be discussed and compared with finite element simulations. For this purpose, normalized load parameters are introduced as:

$$\begin{aligned}&\text{normalized voltage: } V' = V\sqrt{\frac{12\epsilon R^4(1-\nu^2)}{d^6 E}}, \\ &\text{normalized pressure: } P' = P\frac{1-\nu^2}{E}.\end{aligned} \tag{16}$$

In addition, the maximum deflection of the plate is normalized with the initial gap size d.

First, consider the case with no pressure ($P' = 0$). The corresponding deflection deformation is modeled as expressed by Eq. (1). The maximum deflection occurs at the midpoint ($\rho = 0$), and is equal to $C_1 d$.

Fig. 3 shows the change of the midpoint deflection as a function of the applied voltage. The presented curves are determined analytically for different thicknesses of the flexible electrode. The results of the finite element simulations are also shown in this figure, and as can be observed, they confirm the accuracy of the approximate analytical solution. The error between these two solutions in worst case ($h/d = 0.1$) occurs at the limit point and is less than 8%. In fact, the accuracy of the analytical solution is better for thicker electrodes.

As Fig. 3 indicates, the deflection of the midpoint of the flexible electrode increases monotonically with the applied voltage until the system reaches a limit point or saddle-node bifurcation. At this critical point, the system becomes unstable, and if the voltage is increased, it leads to pull-in.

It can be observed from Fig. 3 that the critical defection depends on the thickness of the structure. In fact, solving Eqs. (10) and (11) for $P = 0$, results in a critical deflection ($\frac{w^{cr}}{d} = C_1^{cr}$) which is only a function of h/d. This function is shown in Fig. 4. The critical deflection calculated with the proposed method varies between 51–71% of the initial gap between the electrodes and is always higher than 1/3 of the initial gap which is calculated with a simple 1D spring model. This, as mentioned before, is because modeling the elastic restoring forces with a linear spring does not account for the non-uniform electrostatic force on the

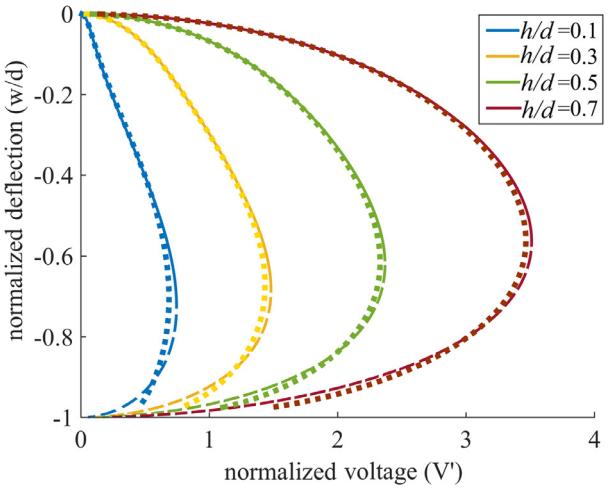

Fig. 3. The equilibrium path of the midpoint of the circular flexible electrode for different thicknesses, and radius $R = 100$ μm. —— stable equilibrium, - - - - unstable equilibrium, and ▪ ▪ ▪ ▪ finite element simulations (COMSOL Multiphysics).

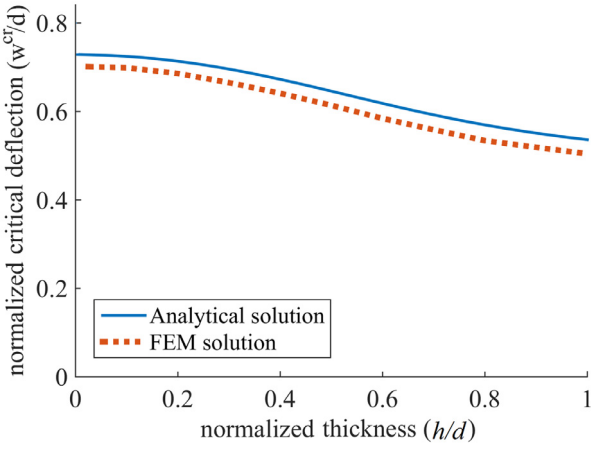

Fig. 4. The normalized critical deflection at the midpoint of a circular plate with radius $R = 100$ μm, as a function of its normalized thickness h/d.

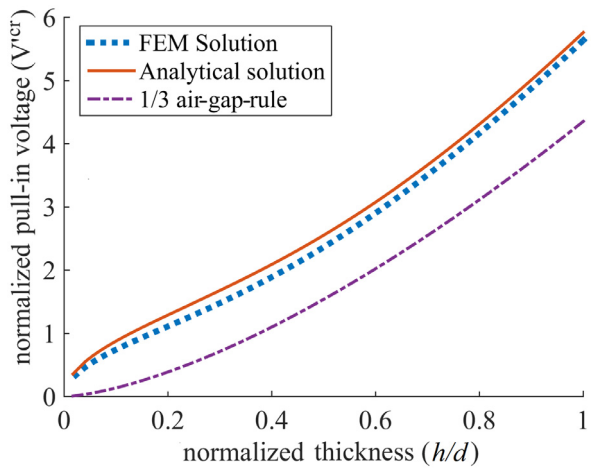

Fig. 5. The normalized pull-in voltage of a circular plate with radius $R = 100$ μm, as a function of its normalized thickness h/d calculated with different methods.

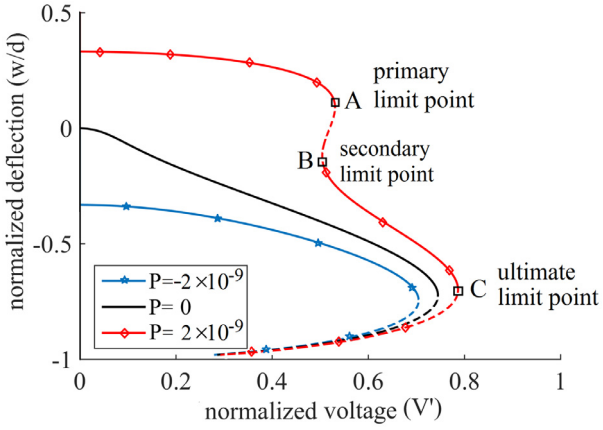

Fig. 6. The midpoint deflection of the circular flexible electrode with thickness $h = 0.2$ μm and radius $R = 100$ μm as a function of applied voltage, for differential pressures in different directions. —— stable equilibrium, - - - - unstable equilibrium.

plate after deflection, and, the nonlinear stiffening effect of the flexible electrode. The latter effect is more pronounced for thinner plates, causing $\frac{w^{cr}}{d}$ to be larger.

The critical voltage of the system, depends on the material properties and the dimensions of the capacitor. Solving Eqs. (10) and (11) for $P = 0$ shows that the pull-in voltage is proportional to $1/R^2$, which is in agreement with the experimental results presented by [44]. The *normalized* critical voltage as defined using Eq. (16), only depends on the normalized thickness, see Fig. 5. For comparison, the finite element results and the results of a simple solution based on 1/3-air-gap theory with uniform electrostatic load (as explained in [12]), are also shown. It is worth to note that the results presented in this graph are closely similar (5% different) to the classical limit provided by Ansari et al. [20]. In the latter, the authors have employed couple stress and strain gradient elasticity theory to obtain the size dependent pull-in characteristics for a micro-plate with $h/d = 0.83$. However, since the geometric nonlinearity is not considered in the mentioned article, the obtained critical deflections are significantly different.

For thinner plates where the nonlinear stiffening effect is more significant, the simple 1D linear spring model (1/3-air-gap rule) predicts a significantly lower critical voltage as compared to the finite element solution; while, the approximate analytical solution presented here can predict very precise results. However, although the critical voltage calculated with the 1D linear spring model is inaccurate for the circular membranes, it provides a more conservative approximation for the critical deflection.

Next, consider the case where a differential pressure, positive in opposing direction of the electrostatic load, is applied ($P' \neq 0$). This time, two load parameters, i.e. pressure and electrostatic load are involved in the stability analysis. In order to calculate the limit voltage, we preserved the pressure and consider the voltage as the varying load parameter. The midpoint deflection of the electrode as a function of applied voltage is shown for three different differential pressures in Fig. 6.

In fact, pressurizing the flexible electrode can significantly affect the shape of the equilibrium path: first of all, a mechanical pressure leads to an initial deflection in the plate when $V = 0$. This initial deflection depends on the amount and direction of the applied pressure. Second, a differential pressure might influence the position and/or number of limit points.

As Fig. 6 shows, when a negative (downward in Fig. 2) pressure is applied, the pull-in voltage drops and the critical deflection slightly increases. This is because a negative differential pressure decreases the average initial distance between the electrodes. Though, the overall shape of the equilibrium path remains the same.

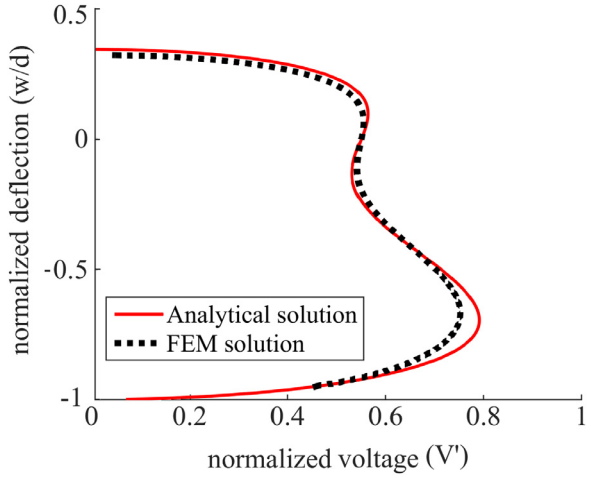

Fig. 7. The midpoint deflection of the circular flexible electrode with thickness $h = 0.2$ μm and radius $R = 100$ μm as a function of applied voltage, when $P' = 2 \times 10^{-9}$.

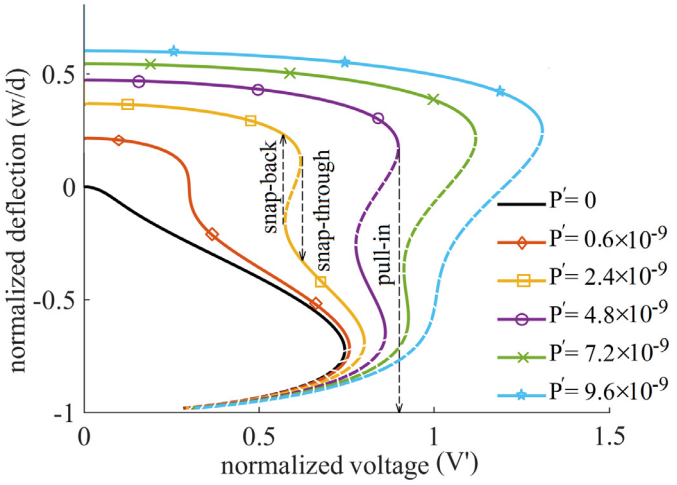

Fig. 8. The midpoint deflection of the circular flexible electrode with thickness $h = 0.2$ μm and radius $R = 100$ μm as a function of applied voltage, for different positive pressures. —— stable equilibrium, - - - - unstable equilibrium.

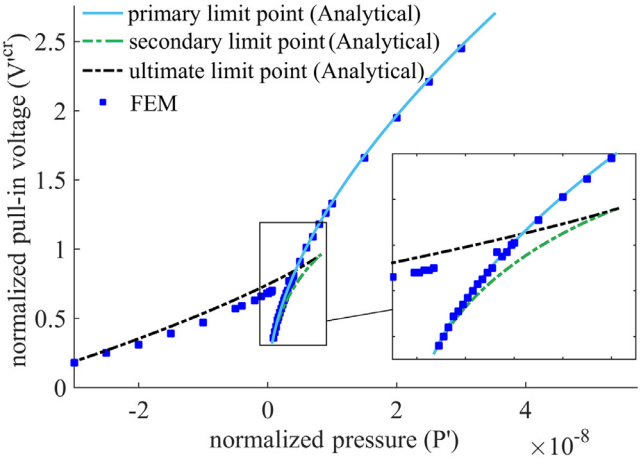

Fig. 9. The critical voltage(s) for a test case with thickness $h = 0.2$ μm and radius $R = 100$ μm, as a function of the applied mechanical pressure.

For positive pressures, however, the shape of the equilibrium path might differ significantly (see $P' = 2 \times 10^{-9}$ in Fig. 6). In such a case, the system exhibits one or three saddle-node bifurcations in its equilibrium path [39]. One limit point (Point C in Fig. 6) is close to the limit point in an unloaded system, i.e. $P' = 0$. Only, due to the initial deflection of the plate and the associated additional geometrical stiffness, this limit point occurs at a slightly different voltage and deflection. We refer to this critical point as the "ultimate" limit point. Another limit point occurs earlier when the deflection of the plate is still in the positive direction (Point A in Fig. 6). We shall refer to this point as the "primary" limit point. The other limit point is a local minimum in the applied voltage (Point B). If we ramp up the voltage on the upper stable branch around Point A, or, ramp down the voltage on the lower stable branch around Point B, the system might jump from one stable configuration to the other.

Similar bi-stability behavior has been observed for shallow arched structures [45]. These structures may exhibit two different stable configurations under the same applied electrostatic load and they can snap from one to the other. For the problem at hand, the pressure is causing the initially flat flexible electrode to behave like an arched structure.

In order to verify the analytical approximate, the equilibrium path calculated by the finite element model is provided in Fig. 7. The results of the numerical solution confirm the accuracy of the approximate analytical solution. The error between these two solutions appears to be the most at the ultimate limit point (approximately 4%). Similar to the case of no pressure, the accuracy of the analytical solution is better for thicker electrodes.

After the system passes the primary limit point, the post-instability behavior strongly depends on the applied pressure. Fig. 8 shows the midpoint deflection as a function of applied voltage, for different positive pressures. It can be observed that the primary limit point can only be noticed if the pressure is higher than a certain threshold. If the applied pressure is too small (see $P' = 0.6 \times 10^{-9}$ in Fig. 8), then, the shape of the equilibrium path changes slightly, and the primary instability is not observed. For higher pressure, though, the primary limit point exists.

For moderate pressures, the primary limit voltage is lower than the ultimate limit voltage. Therefore, the instability leads to the snapping behavior discussed before (see $P' = 2.4 \times 10^{-9}$ in Fig. 8). For larger pressures, the primary critical voltage exceeds the ultimate pull-in voltage and thus, a small perturbation may lead to pull-in of the flexible electrode (see $P' = 4.8 \times 10^{-9}$). For larger pressures, the so-called secondary and ultimate limit points totally vanish.

If during the electrostatic loading, a snap-trough occurs from the upper stable branch to the lower branch (e.g. for $P' = 2.4 \times 10^{-9}$ in Fig. 8), the unloading of the system can also lead to a snap-back from the lower stable branch to the upper one. However, the snap back occurs at a lower voltage at the secondary limit point. This limit point is only observed for the pressure range that both primary and ultimate limit points are present.

Clearly, the critical voltage(s) and limit deflection(s) depend on the applied mechanical pressure. The variation of the limit voltage(s) versus the applied mechanical pressure is shown in Fig. 9. As can be seen, the results of analytical and finite element simulations are in good agreement, which again demonstrates the accuracy of the approximate solution.

In Fig. 9, for negative pressures, only one limit point is observed which is associated with the ultimate limit point or the pull-in of the flexible electrode. In this region ($P' < 0$), there is a near-linear relation between the pull-in voltage and the applied pressure. The pull-in voltage monotonically decreases with increasing the amplitude of the pressure in negative (downward) direction.

For positive pressures, three different regions can be observed. First, for very small pressures, only the ultimate limit point is observed. This is associated with the limit point for $P' = 0.6 \times 10^{-9}$ in Fig. 8. Then, there is a region in which the system exhibits all three limit points. The

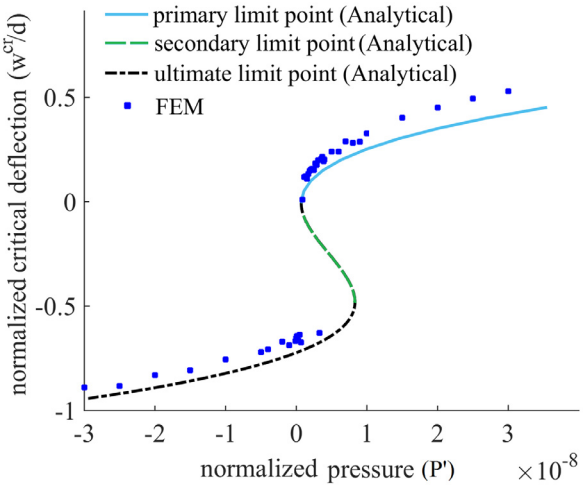

Fig. 10. The critical deflection(s) of the test case with thickness $h = 0.2$ μm and radius $R = 100$ μm, as a function of the applied mechanical pressure.

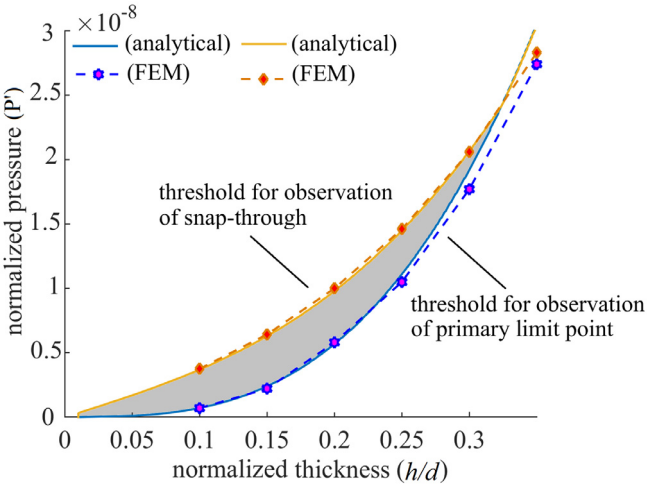

Fig. 11. The pressure range in order to trigger the primary limit point and the snap-through, as a function of thickness of the flexible electrode, with $R = 100$ μm.

examples of $P' = 2.4 \times 10^{-9}, 4.8 \times 10^{-9}$ and 7.2×10^{-9} in Fig. 8 belong to this region. Depending on the value of the applied pressure, the primary limit voltage might be less or more than the ultimate limit voltage. This defines the post-instability behavior of the system. The final region in Fig. 9 is the pressure range at which again the system exhibits only one limit point, which is associated with the so-called primary limit point. The example of $P' = 9.6 \times 10^{-9}$ in Fig. 8 belongs to this region.

Fig. 10 shows how the critical deflections vary with the applied mechanical pressure. It can be observed that the primary critical deflection varies between 0–50% of the initial gap size in the positive direction. At the ultimate pull-in point, the deflection of the plate is 65–73% of the initial gap size.

The snapping of the flat flexible electrode, when sweeping the applied voltage up and down, is an interesting phenomenon that could be used in electrostatically driven switches, sensors and actuators. However, as explained, only a certain range of pressure allows for existence of this behavior. The range of pressures allowing for snapping mainly depends on the mechanical properties of the flexible electrode and its dimensions (thickness and radius).

It should be noticed that snap-through is a dynamic process and when the flexible plate is snapping from an unstable to a stable state, it has nonzero velocity. However, since the load system is conservative, no dynamic consideration is required to assess stability. Instead, the total potential energy is a good criteria to ensure that the dynamic process does or does not lead to failure: *If the total potential energy at the primary limit point exceeds the potential at the ultimate limit point, the exceeding energy appears as kinetic energy causing an overshoot to occur.*

Fig. 11 illustrates the required combination of differential pressure and thickness of the plate, in order to observe the snap-through phenomena. This graph is determined using both analytical and FEM solutions for the test case at hand. The good agreement between the solutions again demonstrates the accuracy of the analytical approximate.

As Fig. 11 shows, if the pressure is too low, the primary limit point is not observed; and if the pressure is too high, then the primary limit voltage exceeds the ultimate limit voltage and the system would fail after reaching the first instability.

If the pressure is high enough, the ultimate and secondary limit points vanish and snap-back behavior will not be observed either. However, one can conclude from Figs. 8 and 9 that the pressure range for having snap-through in loading is a subset of the range for having the snap-back in unloading. In fact, if the snapping in loading is observed, the occurrence of snap-back in unloading is certain.

Fig. 12 shows the admissible combinations of the applied pressure and thickness for existence of snapping, for different radii of the electrode. As can be observed for smaller radii of the electrode (for example, $R/d = 40$ in Fig. 12) a wide range of pressures might result in snap-through behavior. However, for larger electrodes the range of admissible pressures drops. It is interesting that the required thickness, resulting in snap-through, is always less than 33% of the gap size. For a thicker electrode, the primary instability, if observed, leads to direct pull-in.

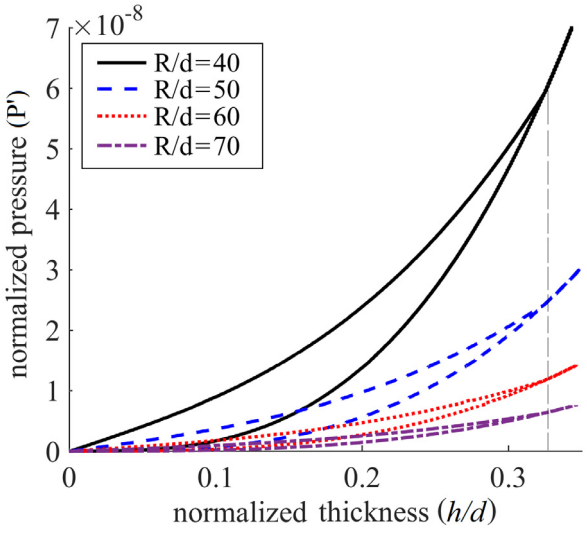

Fig. 12. The pressure range in order to trigger the primary limit point and the snap-through, as a function of thickness of the flexible electrode, for different radii.

Although the snap-through has been illustrated for constant pressures and a varying voltage, a similar behavior will be observed if the voltage is preserved and the pressure is varied. The midpoint deflection of the electrode as a function of the applied pressure, for different voltages, is provided in Fig. 13. It can be observed from Fig. 13 that for any voltage larger than zero, at least one limit point exists in the equilibrium path (e.g. Point A for V'= 0.45). However, for larger voltages, two other limit points might appear. For example, in Fig. 13, in the curve corresponding to V'= 0.45, if we vary the pressure around Point B or C, the system snaps from a positive to a negative deflection, or vice versa. For very large voltages, on the other hand, varying the pressure over the limit points leads to pull-in of the system.

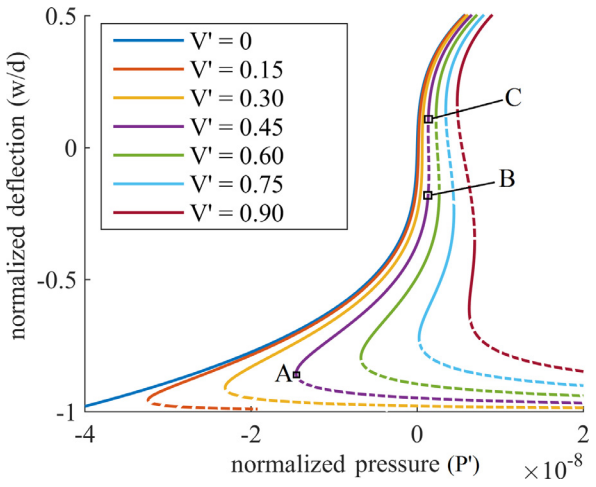

Fig. 13. The midpoint deflection of the circular flexible electrode with thickness $h = 0.2$ μm and radius $R = 100$μm as a function of the applied pressure. —— stable equilibrium, - - - - unstable equilibrium.

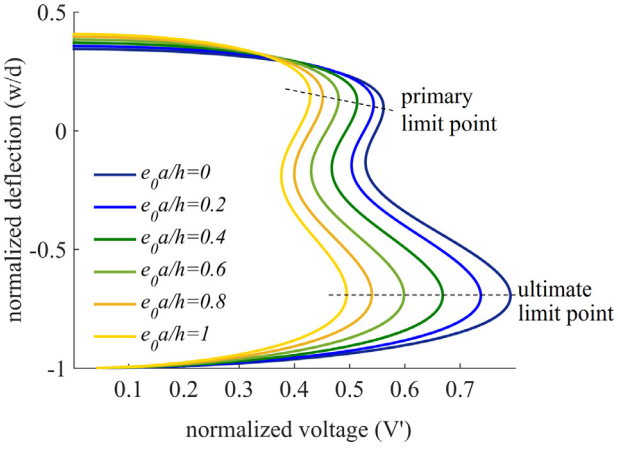

Fig. 14. The midpoint deflection of the circular flexible electrode obtained by nonlocal continuum theory with different material length scales as a function of applied voltage, for $h = 0.2$ μm, $R = 100$ μm, and $P' = 2 \times 10^{-9}$.

It is worth to point out that the compliance of the system to a differential pressure is minimum in case no voltage is applied to the capacitor. With a voltage increase the stiffness of the system drops, and finally at a critical voltage, the system allows for snap-through behavior. When snap-through occurs, the system has zero stiffness. The snap-through and bi-stable behavior noticed for pressurized clamped electrodes, can be employed in sensing and actuation applications. This phenomenon can benefit from high sensitivity due to low compliance, and robustness and simplicity of pull-in voltage measurements.

Finally, it should be noted that the hypothetical properties that were utilized for illustrating the results are close to those of gold or aluminum thin films. For these two materials, scale effects are not significant at the thicknesses used in the present study [26–29]. Therefore, provided that we restrict the material to aluminum and gold or other similarly behaving materials, the classical continuum theory can be employed at the discussed length scales. However, for smaller length scales, a size-dependent continuum theory shall be utilized. Here, we briefly show the results of using a nonlocal plate theory together with the proposed formulation to capture the effects of scaling on assessment of the stability of the micro-plate. Fig. 14 shows how the predicted size dependent deflection varies with the applied voltage. For comparison the results for different material length scales from classical limit ($e_0a/h = 0$) to the limit of application of the nonlocal theory ($e_0a/h = 1$) are illustrated in this graph. It can be observed that the three limit points (primary, secondary and ultimate limit points) still exist in the equilibrium path of the micro-plate obtained by non-local theory. This figure shows that when the thickness of the micro-plate gets comparable to the material length scale, (i) the initial deflection increases, (ii) the critical voltages decrease, and (iii) the critical deflections slightly increase. It is noteworthy that these results are qualitatively in agreement with the results provided by Ref. [30] which investigates the size-dependent dynamic pull-in analysis of micro-plates using modified couple stress theory.

6. Conclusions

In this paper, an analytical model was proposed for a circular flexible electrode in a parallel plate capacitor, while it is loaded with a differential pressure. Using this approximate solution, a stability analysis was performed on the effect of pressure on the critical voltage and deflection. In the proposed model, the geometrical non-linearity of the flexible electrode was taken into account.

The results suggest that a pressure can trigger additional limit points and an unstable solution branch to occur. The post-instability behavior after reaching the first limit point, depends on load parameters, thickness and radius of the electrode and the air gap. After the primary limit point, the system might snap to a new stable configuration, or, exhibit pull-in.

It is worth to mention here that when snap-through occurs, the system has very small stiffness, and is mechanically very compliant. This condition makes the system very suitable for sensing applications. In particular, the sensitivity of the limit voltages to the pressure can be employed to measure the pressure. However, we stress here that even without observation of instability, the combination of positive pressure and electrostatic load on the flexible electrode results in a high compliance of the system, which may be very appealing for sensing applications.

Moreover, to capture the size dependency of stability of a micro-plate while loaded with electrostatic and differential pressures, a formulation in framework of nonlocal continuum theory has been suggested. This formulation includes the scaling effects of the thickness of the micro-plate and hence, it is suitable for being used for smaller length scales where the application of classical continuum theory is limited. The results of the size-dependent model exhibit similar aspects of the mechanical behavior of the plate such as the additional limit points and snap-through behavior. Consequently, the demonstrated behavior could serve as a basis for novel micro as well as *nano* electro mechanical systems. Using the primary instability of pressurized electrodes in sensing or actuation can benefit from the robustness and simplicity of pull-in measurements, and in addition, it can benefit from the snap-through behavior which prevents the system from failure.

Acknowledgment

This work is supported by NanoNextNL, a micro and nanotechnology consortium of the Government of the Netherlands and 130 partners.

References

[1] Krylov S, Ilic BR, Schreiber D, Seretensky S, Craighead H. J Micromech Microeng 2008;18(5):055026. doi:10.1088/0960-1317/18/5/055026.
[2] Zhang W-M, Yan H, Peng Z-K, Meng G. Sens Actuat A 2014;214:187–218. doi:10.1016/j.sna.2014.04.025.
[3] Vogl GW, Nayfeh AH. A reduced-order model for electrically actuated clamped circular plates. In: ASME 2003 international design engineering technical conferences and computers and information in engineering conference. American Society of Mechanical Engineers; 2003. p. 1867–74. doi:10.1088/0960-1317/15/4/002.
[4] Khater M. Use of instabilities in electrostatic micro-electro-mechanical systems for actuation and sensing; 2011. Thesis.
[5] Smyth KM. Design and modeling of a PZT thin film based piezoelectric micromachined ultrasonic transducer (pmut); 2012. Thesis. URL: http://hdl.handle.net/1721.1/74942.

[6] Chuang W-C, Lee H-L, Chang P-Z, Hu Y-C. Sensors 2010;10(6):6149–71. doi:10.3390/s100606149.
[7] Elata D, Abu-Salih S. J Micromech Microeng 2005;15(5):921. doi:10.1088/0960-1317/15/5/004.
[8] Sajadi B., Alijani F., Goosen H., van Keulen F.. Static and dynamic pull-in of electrically actuated circular micro-membranes. In: ASME 2016 international mechanical engineering congress and exposition. American Society of Mechanical Engineers; p. V04AT05A030–V04AT05A030. 10.1115/IMECE2016-67336
[9] Liao L-D, Chao PC, Huang C-W, Chiu C-W. J Micromech Microeng 2010;20(2):025013. doi:10.1088/0960-1317/20/2/025013.
[10] Sadeghian H, Yang C-K, Goosen H, Van Der Drift PJF, Bossche A, French PJF, et al. Appl Phys Lett 2009;94(22):221903–221903–3. doi:10.1063/1.3148774.
[11] Sadeghian H, Goosen H, Bossche A, van Keulen F. Thin Solid Films 2010;518(17):5018–21. doi:10.1016/j.tsf.2010.03.036.
[12] Lardiès J, Berthillier M, Bellaredj ML. Analytical investigation of the pull-in voltage in capacitive mechanical sensors. SPIE microtechnologies. International Society for Optics and Photonics; 2011. doi:10.1117/12.887460. 80661N–80661N–10.
[13] Sharma A, George PJ. Sens Actuat A 2008;141(2):376–82. doi:10.1016/j.sna.2007.10.036.
[14] Osterberg PM, Senturia SD. M-Test: a test chip for mems material property measurement using electrostatically actuated test structures. Microelectromech Syst J 1997;6(2):107–18. doi:10.1109/84.585788.
[15] Cheng J, Zhe J, Wu X, Farmer KR, Modi V, Frechette L. Analytical and fem simulation pull-in study on deformable electrostatic micro actuators. In: Technical proc. of the international conf on modeling and simulation of microsystems, MSM; 2002. p. 298–301. ISBN 0-9708275-7-1, URL: http://www.nsti.org/procs/MSM2002/5/W51.21.
[16] Duan G, Wan K-t. Int J Mech Sci 2010;52(9):1158–66. doi:10.1016/j.ijmecsci.2010.04.005.
[17] Sadeghian H, Yang C-K, Goosen H, Bossche A, French PJF, Van Keulen F. Sens Actuat A 2010;162(2):220–4. doi:10.1016/j.sna.2010.01.012.
[18] Sharma J, Dasgupta A. J Micromech Microeng 2009;19(11):115021. doi:10.1088/0960-1317/19/11/115021.
[19] Krylov S, Seretensky S. J Micromech Microeng 2006;16(7):1382. doi:10.1088/0960-1317/16/7/036.
[20] Ansari R, Gholami R, Mohammadi V, Shojaei MF. J Comput Nonlinear Dyn 2013;8(2):021015. doi:10.1115/1.4007358.
[21] Sajadi B, Goosen J, van Keulen F. Appl Phys Lett 2017;111(12):124101–1–5. doi:10.1063/1.5003223.
[22] Sajadi B, Alijani F, Goosen H, van Keulen F. Nonlinear Dyn 2017:1–14.
[23] Nabian A, Rezazadeh G, Haddad-derafshi M, Tahmasebi A. Microsyst Technol 2008;14(2):235–40. doi:10.1007/s00542-007-0425-y.
[24] Comsol multiphysics user guide (version 4.3 a). 2012. URL: www.comsol.nl.
[25] Sadeghian H, Goosen H, Bossche A, Thijsse B, van Keulen F. On the size-dependent elasticity of silicon nanocantilevers: impact of defects. J Phys D Appl Phys 2011;44(7):072001. doi:10.1088/0022-3727/44/7/072001.
[26] Espinosa H, Prorok B. J Mater Sci 2003;38(20):4125–8.
[27] Oh H-J, Kawase S, Hanasaki I, Isono Y. Jpn J Appl Phys 2014;53(2):027201. doi:10.7567/JJAP.53.027201.
[28] Haque M, Saif M. Proc Natl Acad Sci USA 2004;101(17):6335–40.
[29] Haque M, Saif MA. Scr Mater 2002;47(12):863–7. doi:10.1016/S1359-6462(02)00306-8.
[30] Askari AR, Tahani M. Size-dependent dynamic pull-in analysis of geometric non-linear micro-plates based on the modified couple stress theory. Physica E 2017;86:262–74.
[31] Asghari M. Int J Eng Sci 2012;51:292–309. doi:10.1016/j.ijengsci.2011.08.013.
[32] Rahaeifard M, Kahrobaiyan M, Asghari M, Ahmadian M. Sens Actuat A 2011;171(2):370–4.
[33] Asghari M, Kahrobaiyan M, Ahmadian M. Int J Eng Sci 2010;48(12):1749–61. doi:10.1016/j.ijengsci.2010.09.025.
[34] Asghari M, Rahaeifard M, Kahrobaiyan M, Ahmadian M. Mater Des 2011;32(3):1435–43. doi:10.1016/j.matdes.2010.08.046.
[35] Sajadi B, Goosen H, van Keulen F. Int J Solids Struct 2017. doi:10.1016/j.ijsolstr.2017.03.010.
[36] Asghari M, Ahmadian M, Kahrobaiyan M, Rahaeifard M. Mater Des 2010;31(5):2324–9. doi:10.1016/j.matdes.2009.12.006.
[37] Zhao M, Slaughter WS, Li M, Mao SX. Acta Mater 2003;51(15):4461–9.
[38] Eringen AC. Nonlocal continuum field theories. Springer; 2002. doi:10.1007/b97697. ISBN 0387952756
[39] Amabili M. Nonlinear vibrations and stability of shells and plates. Cambridge University Press; 2008. doi:10.1017/CBO9780511619694. ISBN 1139469029
[40] Timoshenko S, Woinowsky-Krieger S, Woinowsky S. Theory of plates and shells, 2. McGraw-hill New York; 1959. URL: https://books.google.nl/books?id=rTQFAAAAMAAJ.
[41] Sajadi B, Alijani F, Davidovikj D, Steeneken PG, Goosen H, van Keulen F. J Appl Phys 2017;in press.
[42] Lu P, Zhang P, Lee H, Wang C, Reddy J. Proc R Soc A 2007;463(2088):3225–40. doi:10.1098/rspa.2007.1903.
[43] Eringen AC. J Appl Phys 1983;54(9):4703–10. doi:10.1063/1.332803.
[44] Osterberg PM. Electrostatically actuated microelectromechanical test structures for material property measurement; 1995. Thesis. URL: http://hdl.handle.net/1721.1/11097.
[45] Das K, Batra RC. Smart Mater Struct 2009;18(11):115008. doi:10.1088/0964-1726/18/11/115008. URL: http://iopscience.iop.org/0964-1726/18/11/115008.